SYSTEM SAFETY: HUMAN - TECHNICAL FACILITY – ENVIRONMENT
6(1), 2024, pp. 473-484

VARIOUS METALLOGRAPHY TECHNIQUES FOR MICROSTRUCTURE ANALYSIS OF Ni-BASED SUPERALLOYS

DOI: 10.2478/czoto-2024-0048
Received: 12/11/2024
Accepted: 30/12/2024

Juraj Belan[1] – *orcid id: 0000-0002-2428-244X, e-mail: juraj.belan@fstroj.uniza.sk*
Milan Uhríčik[1] – *orcid id: 0000-0002-2782-5876, e-mail: milan.uhricik@fstroj.uniza.sk*
Martin Mikolajčík[1] – *orcid id: 0000-0002-7477-6237, e-mail: martin.mikolajcik@fstroj.uniza.sk*
Zuzana Šurdová[1] – *orcid id: 0000-0002-4823-2279, e-mail: zuzana.surdova@fstroj.uniza.sk*
[1]University of Žilina, Faculty of Mechanical Engineering, Department of Materials Engineering, Univerzitná 8215/1, 01026 Žilina, **Slovakia**

Abstract: The Ni-based superalloys are known for the number of phases presented in alloy microstructure. Depending on alloying elements, phases such as austenitic FCC gamma matrix, L_{12} gamma prime, DO_{22} gamma double prime, BCT delta phase, and MC or $M_{23}C_6$ (or M_6C) carbides have occurred. With these microstructure components' variety, the usual optical microscopy analysis is not satisfactory many times. For a better understanding of how single structures affect the lifetime of Ni-based superalloys components (turbine blades or turbine discs) and how they are changing during their operation load is SEM a very powerful tool. Two different types of superalloys were used for experimental evaluation. The first were cast superalloys ZhS6K and IN 738. Both cast superalloys in bar form were subjected to additional heat treatment at 800°C for 10 and 15 hours followed by air-cooling. The influence of gamma prime phase morphology changes on alloy lifetime and Vickers hardness were evaluated by SEM coherent testing grid methods. The second was wrought superalloy IN 718 and Nimonic 80A in bar form to present the various grain size evaluation techniques according to ASTM E112 standards. Various analyses were employed (SEM fractography, BSE observation, EDS mapping, etc.) for microstructure evaluation. The main goal is to show how effective light microscopy and SEM on Ni-based superalloy analysis are when microstructure change evaluation is needed.
Keywords: Ni-based superalloys, optical microscopy, SEM analysis, gamma prime phase, delta phase, grain size evaluation

1. INTRODUCTION

Superalloys are classified according to the main alloying elements in the composition, with the three base metals being nickel, cobalt, and iron. The entire superalloy family

shares a common basic microstructure, which is a face-centered cubic (FCC) matrix with a number of dispersed secondary strengthening phases. In elemental form, nickel is the only superalloy base metal with an FCC structure at room temperature. Cobalt is hexagonally close-packed (HCP) at room temperature but undergoes a transformation to FCC at 417°C. Iron has a body-centered cubic (BCC) structure at room temperature but undergoes a phase transformation to FCC austenite at 912°C. In superalloys, both iron and cobalt are stabilized by the addition of nickel to retain an FCC crystal structure throughout the gas turbine engine (GTE) application temperature range (Gaddes et al. 2010).

Ni-Fe-base superalloys are characterized by their high toughness and ductility and are used mostly in applications where these properties are required, such as turbine discs or forged rotors. Consequently, Ni-Fe alloys are used only in the wrought condition, because this manufacturing method offers a wide variety of mechanisms for controlling grain size and morphology (Donachie and Donachie, 2002). There are three groups of Ni-Fe-base superalloys. The first is the precipitation - hardened alloys discussed subsequently, where γ'-Ni_3(Al, Ti) and/or γ''-Ni_3Nb precipitates form in the FCC γ matrix. The second is the low-coefficient-of-thermal-expansion (CTE) group of alloys. The third group of nickel-iron-base superalloys is the modified stainless steels, primarily strengthened by solid-solution hardening and minor carbide precipitation.

Among the alloys that are strengthened through γ' precipitation are A-286, V-57, Nimonic 901, and Inconel 718. Unfortunately, γ' precipitation only occurs at low levels of aluminum in Ni-Fe-base alloys, which means that most Ni-Fe-base superalloys rely on titanium additions for hardening through the precipitation of γ'-Ni_3Ti. Long-term exposure above 650°C tends to cause the γ' to transform to coarse platelet η phase (an HCP Ni_3Ti phase), which results in a considerable decrease in strength (Durand-Charre, 1997). Low levels of Al also decrease the environmental resistance of the alloy, because without sufficient Al, the alloy cannot form a protective Al scale. Another highly effective strengthening precipitate, body-centered tetragonal γ''-Ni_3Nb, forms in alloys that contain Nb. The most widely known such alloy is Inconel 718, a highly weldable superalloy, which accounts for 35% of total wrought superalloy production worldwide (Manriquez et al., 1992). It is used in aircraft GTE components such as the compressor and turbine discs, casings, compressor blades, and fasteners. Some alloys may contain combined Al, Ti, and Nb, which could result in dual strengthening by γ' and γ'', as is the case with Inconel alloys 706, 709, and 718. These three alloys may be considered to be Ni-base, but they have sufficiently high Fe contents to be classified as Ni-Fe-base superalloys.

Ni-base superalloys achieve the highest temperature/strength combination of all cast and wrought superalloys, making them ideal for the most demanding applications, such as turbine blades. Wrought Ni-base superalloys are often used where high toughness is required, such as turbine discs and forged blades. Examples of the wrought alloys include Udimet 700, Rene 41, Waspaloy, N-901, and Udimet 630. Castings are favored for high strength and creep resistance in high-temperature applications, such as investment-cast turbine blades and wheels, and are represented by alloys such as Inconel alloys 100, 713, 738, and 792, B-1900, and MAR-M 200 and single-crystal cast alloys PWA1483, PWA1484, CMSX-4, and Rene N6. The

superior high-temperature capability of nickel-base superalloys is due to the precipitation of high volume fractions of the γ'-Ni_3(Al, Ti) phase, which requires combined Al and Ti contents of at least four to six weight percent. This precipitate is the main strengthening phase in such wrought alloys as Waspaloy, Astroloy, Udimet alloys 700 and 720 and in such cast alloys as Rene 80, MAR-M 247, and Inconel 713 and in all of the directionally solidified and single-crystal superalloys.

Most polycrystalline Ni-base superalloys possess microstructures consisting of ordered intermetallic precipitates γ' ($L1_2$) and/or γ'' ($D0_{22}$) distributed coherently within a disordered γ (FCC) matrix (Donachie and Donachie, 2002, Durand-Charre, 1997, Sims et al., 1987, Pollock and Tin, 2006, Reed, 2006). The remarkable high temperature mechanical properties associated with Ni-base superalloys largely rely on this two – phase microstructure, which provides substantial order and coherency strengthening that hinder the movement of dislocations during deformation. Modern polycrystalline Ni-base superalloys often contain intermediate levels of Al, Ti and Nb to yield an optimized volume fraction of strengthening phase (γ'/γ''), as well as controlled concentrations of refractory elements (W, Mo) to deliver further solid solution strengthening to the γ matrix and the precipitates (Furrer and Fecht, 1999).

There are many phases presented in the microstructure of superalloys; most of them are very fine one, hardly observed with regular optical microscopy (OM) method, neither to identify them. From that reason are various metallography techniques used for identification as well as observation of such phases. The easiest way to identify phases, especially carbides, γ/γ' eutectic cells, grains size (or grains identification as it self), is color etching or color contrast developing via color chemical reagents (etchants). However, here we are limited by optical microscope magnification and resolution as well. Therefore, techniques of SEM are more helpful and provide more sophisticated information when using a proper tool for phases observing and identifying, like back scattered electron (BSE), microanalysis of chemical composition by use of EDS detector attached to the SEM (EDS techniques - mapping or line). The positive advantage of SEM is that need no special chemical treating of specimens (also deep etching or selective etching techniques can be useful). This contribution shows how useful tool can SEM analysis be when superalloys phases need to be evaluated.

2. EXPERIMENTAL MATERIALS AND METHODS

Four Ni-based superalloys used. Two of them are in as cast condition, namely superalloy signed as ZhS6K and further, Inconel's alloy 738C. The third one is well known and the constructor most favorite wrought Inconel's alloy 718 and the forth is Nimonic alloy 80A – a wrought, age-hardenable Ni-Cr alloy, strengthened by additions of Ti, Al, and C, developed for service at temperatures up to 815°C. The nominal chemical composition obtained by *SPECTROMAXx* (in wt. %) of alloys is in Table 1.

Ni-based superalloy ZhS6K can be roughly compared to Nimonic group alloys. It is precipitation-hardened alloy with γ' (Ni_3Al gamma prime) fine fractions in γ super-saturated solid solution (Belan et al., 2017). A typical microstructure of as cast alloy with significant dendritic segregation and carbides situated in inter-dendritic areas is on Fig. 1.

Table 1
The chemical composition (in wt. %) of alloys used at experimental work

Alloy	C	Co	Cr	Al	Ti	Nb	W	Mo	Fe	Ta	Ni
ZhS6K*	0.20	4.8	12.4	5.2	3.0	0.01	5.3	3.5	0.2	-	Bal.
IN 738C*	0.17	8.5	16.0	3.4	3.4	0.9	2.6	1.7	0.05	1.75	Bal.
IN 718**	0.026	0.14	19.3	0.57	0.96	5.3	-	3.0	Bal.	0.01	53.32
Nimonic 80A	0.10		22.8	1.28	2.65				0.62		Bal.

Note: * for cast superalloys is Ni content as balance; ** for wrought superalloy is Fe content as balance (own analysis)

a) b)

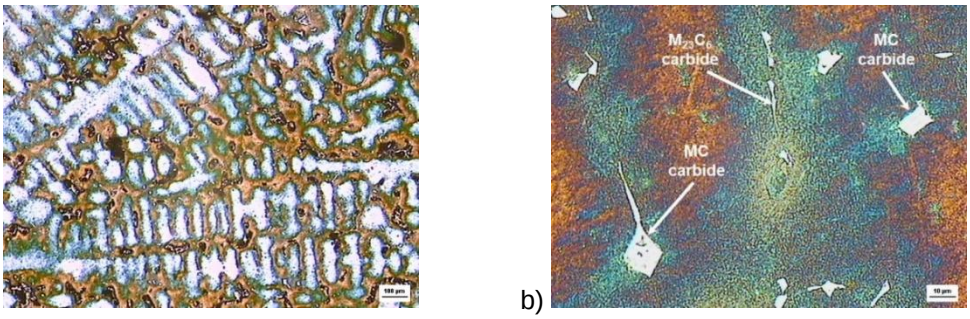

Fig. 1. Optical microscopy microstructures of as cast ZhS6K alloy; a) dendritic segregation, b) carbides at inter-dendritic areas, etch. Beraha III and DIC

Alloy IN738 is a vacuum melted, vacuum cast, precipitation hardenable Ni-based alloy possessing excellent high-temperature creep-rupture strength combined with hot corrosion resistance superior to that of many high-strength superalloys of lower chromium content. It is designed to provide the gas turbine industry with an alloy, which will have good creep strength up to 980°C combined with the ability to withstand long-time exposure to the hot corrosive environments associated with the engine. Our experimental material is high carbon version IN 738C with microstructure represented on Fig. 2. Inconel alloy 718 is a high-strength, corrosion-resistant, and hardenable Ni – Cr alloy with good tensile, fatigue, creep, and rupture strength what have resulted in its use in a wide range of applications. It is used at temperature ranging from -250°C up to 705°C. The strength of the alloy 718 comes from coherent solid-state precipitates, which are for a small part γ'-Ni_3Al but mostly γ''-Ni_3Nb precipitates (Sundararaman et al., 1992, Dehmas et al., 2011). Microstructures are on Fig. 3. NIMONIC 80A superalloy (Fig. 4) is a ductile Ni-based alloy (min. 65% Ni) containing Cr (20%) with small additions of C, Co, and Fe. A polycomponent alloy has acquired its characteristic microstructure and strength after precipitation hardening. Precipitation hardening is caused by the formation of an intermetallic precipitate γ'- $Ni_3(Al, Ti)$ phase. This superalloy was first discovered at the beginning of World War II in Great Britain, where the International Nickel Co. developed it. It is designed for operations with temperature up to 815°C. It is produced by high frequency melting, casting into molds and then cooling in air. Currently, NIMONIC 80A superalloys are used as components for gas turbines (blades, discs, bolts, rings, etc.) and in the automotive industry as part of exhaust systems (Sunulahpašić et al., 2012).
Metallography specimens were prepared by cutting on MTH Micron 3000 precise saw then mounting into bakelite mixture in Struers Cito-Press 1 and finally grinded and

polished with using of Struers Tegra-System (TegraPol-15 and TegraForce-1). Grinding and polishing consist of a few steps; grinding with SiC sand paper No. 320, followed by medium polishing with MD-Allegro and fine polishing with OP-S lubricant. This procedure was applied on specimens for optical microscopy (OM) and for scanning electron microscopy (SEM) and EDS analysis as well. The OM was used for color etched specimens evaluation (dendrite segregation, grain size). OM color etching is useful for quick identification of dendritic segregation and carbide particles became more pronounced. In addition, grain boundaries are more visible what helps to grain size evaluation.

a) 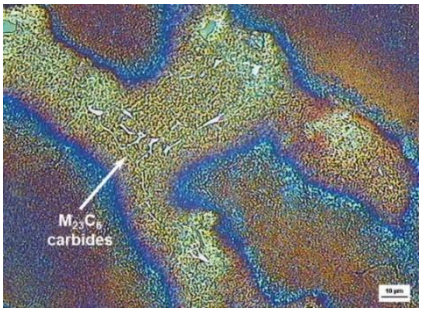

b) 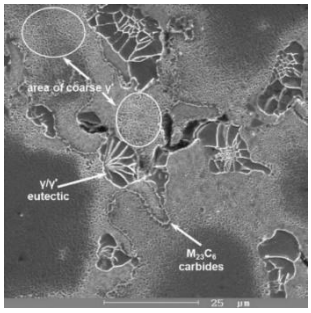

Fig. 2. a) Optical microscopy microstructure of as cast IN 738C alloy dendritic segregation, carbides at inter-dendritic areas, etches. Beraha III and DIC, b) SEM micrograph showing γ/γ′ eutectic cells, secondary $M_{23}C_6$ carbides and areas with coarse γ′ phase situated at inter-dendritic areas, etches. Marble

a) 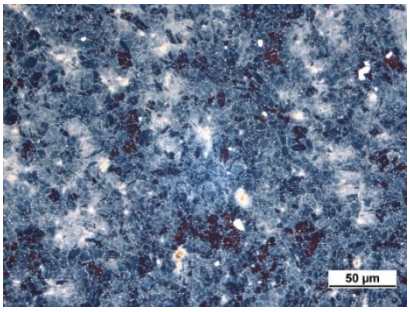

b) 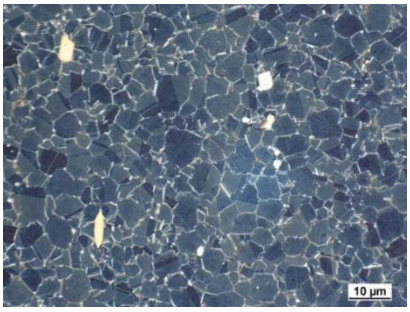

Fig. 3. Optical microscopy microstructures of wrought IN 718 alloy; a) grains in microstructure, according to ASTM E 112/2010 is ASTM 12 (5.6 µm), b) crystallization and deformation twins; etch. Beraha III and DIC

a) 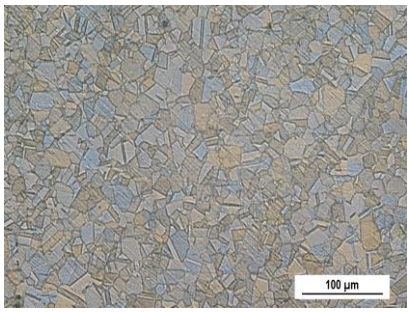

b) 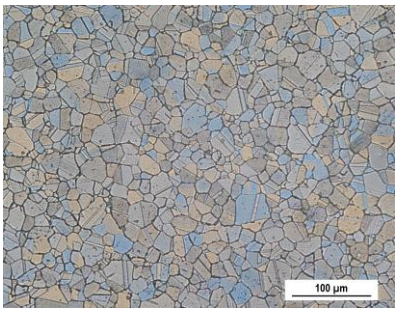

Fig. 4 Microstructure of Nimonic 80A – optical microscopy: a) longitudinal section of the investigated sample, b) transverse section of the investigated sample, etch. Marble + DIC

After specimen preparation were following methods for phase identification and evaluation used:

- Phase identification was done by EDS line analysis and EDS chemical elements mapping. In some specific situation even EDX analysis was employed;
- For the number of γ'-phase particles, a coherent testing grid with 9 square shape area probes on SEM micrographs was used;
- For the volume of γ'-phase particles, a coherent testing grid with 50 dot probes made from backslash crossing on SEM micrographs was used.

For the evaluation of the γ- and γ'-phases the method of coherent testing grid was used, and the number of γ' "N" was evaluated by a grid with 9 square-shaped area probes and the volume of γ' "V" was evaluated by grid with 50 dot probes. For a detailed description of the methods used, see (Vaško, 2016, Belan, 2012). The size of γ' is also important from the point of view of creep rupture life. A precipitate with a size higher than 0.8 μm can be considered heavily degraded and as causing decreasing mechanical strength at higher temperatures.

Note that γ' phase can be evaluated only at ZhS6K or IN 738 cast alloys due to both alloys are strengthened by this precipitating phase. Wrought alloy IN 718 is principal strengthened by γ'' phase and γ' phase become more visible and coarse after sufficient heat-treatment or higher temperature loading (Belan, 2012).

The grain size of wrought IN 718 was evaluated by the planimetric (Jeffries`) method (according to ASTM E112-12). Nimonic 80A was evaluated by two different methods described in ASTM E112-12. The first was the planimetric (Jeffries`) method with a rectangular area of 5000 mm^2; the second was the Heyn linear method with a length of the evaluation lines of 500 mm. The grain size evaluation was performed on the superalloy in its initial state, as delivered by the distributor BIBUS Metals s.r.o. CZ. The microstructure of the samples was observed using an optical microscope using polarized light and DIC techniques.

3. RESULTS AND DISCUSSION

The optical microscopy, as was mentioned above, is not always providing satisfactory phase determination in superalloys. That is the reason to use SEM techniques to get more precise phase identification. There are two methods to determine phases, the line analysis and chemical elements mapping respectively. To confirm carbide particles presence in IN 718 superalloy was line analysis used and results are presented on Fig. 5. Upon this analysis is clear to see, that particle is a primary carbide MC type – namely NbC or TiC – in this particular case is TiC primary carbide type.

For confirming this chemical mapping was used too, Fig. 6a-b, it can be seen even that carbides rich on Nb content are light grey color (at EDS mapping actually yellow one) rounded particles and carbides rich on Ti content are sharp-edged dark grey particles (at EDS mapping are red colored).

The same procedures were used for cast Ni-based ZhS6K superalloy used, Fig. 7, with describing even chemical elements distribution in cross-section. These cast superalloys are typical for its chemical heterogeneity represented by significant dendritic crystallization. Fig. 7a shows overall view on microstructure, where dark areas are paths of primary dendritic areas, which crystallized as first during solidification. This are is characterized with very fine

γ' - Ni_3Al (the Ti content in this strengthening phase is questionable due to high relation of Ti to carbon, therefore Ti mainly goes to primary carbides TiC) phase and interesting fact, no carbide presence in this area. All carbides, no matter if primary MC or secondary $M_{23}C_6$ are situated in inter-dendritic areas when also coarse γ' - Ni_3Al is presented. The Figs. 7b-c shows the elements distribution.

Superalloys are strengthened through three principal mechanisms: a) solid-solution hardening (SSH), b) precipitation hardening (PH), and c) oxide-dispersion strengthening (ODS). For superalloys discussed in this article are the first two strengthening mechanisms the most important. From that reason only them will be further closer described.

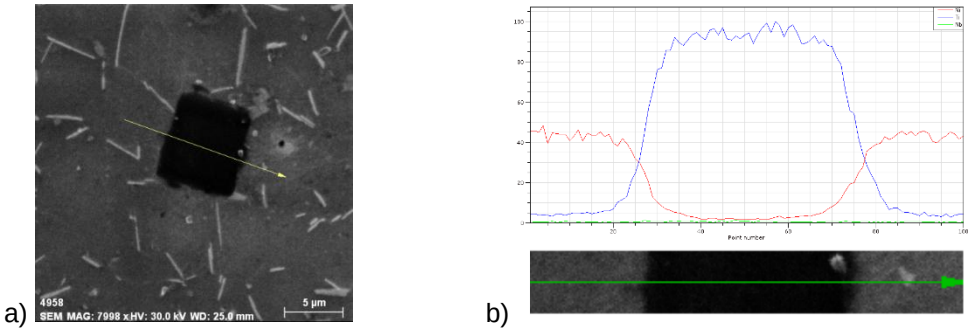

Fig. 5. EDS line analysis of carbide phase in alloy IN 718, a) overall view, b) line analysis, electrolytic etch. 10gCrO_3+100ml H_2O

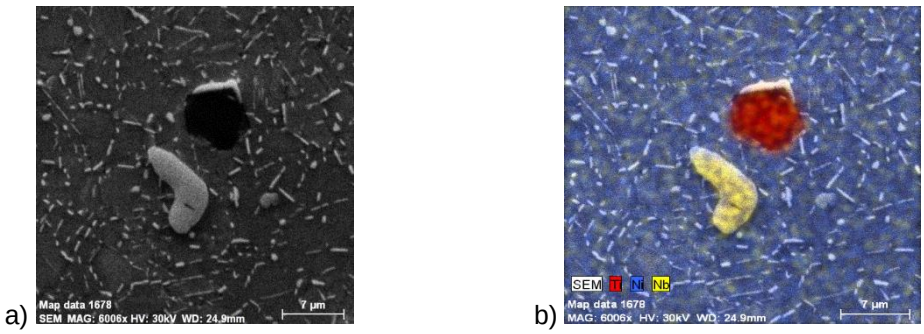

Fig. 6. EDS chemical elements mapping, alloy IN 718, a) overall view, b) carbide particles identification, etch. Marble

Solid-solution hardening is the attainment of an increase in matrix strength by the addition of a different soluble element. The distortion of the atomic lattice caused by the misfit of atomic radius inhibits dislocation movement. Solid-solution hardening increases with atomic size difference, up to a maximum difference of approximately 10% in atomic size (Durand-Charre, 1997). The use of high-melting-point elements as the solutes provides stronger lattice cohesion and reduces diffusion, particularly at high temperatures. Similar considerations apply to the hardening of the γ'- phase. Solid-solution hardening also has the effect of decreasing the stacking fault energy (SFE) in the crystal lattice, leading primarily to inhibition of dislocation cross slip, which is the main deformation mode in imperfect crystals at elevated temperatures (Kumar, 1994). A lower SFE makes it more difficult for dislocations to change directions; thus, when a dislocation encounters a barrier, it is more difficult for the dislocation to be able to bypass that barrier by moving onto a new slip plane (Donachie and Donachie, 2002). In face-centered cubic (FCC) structures, the lowering of SFE leads to three interrelated effects:

- Dissociation of dislocations into partials.
- Formation of hexagonally close-packed (HCP) stacking fault ribbons.
- Increased difficulty of passage of dislocations from FCC matrix to HCP fault.

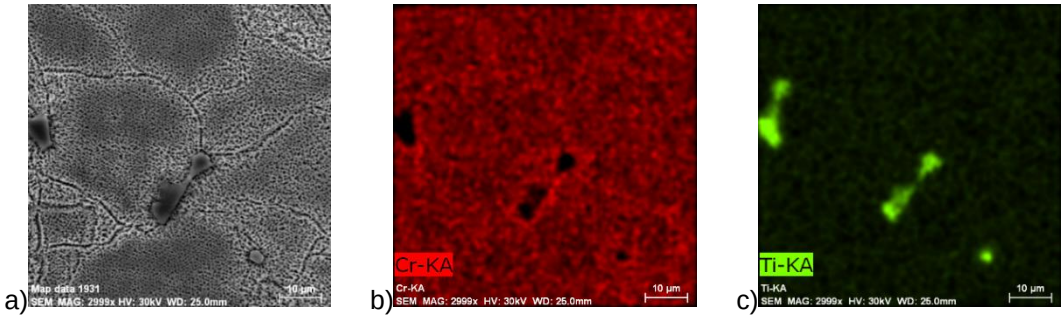

Fig. 7. Ni-based superalloy ZhS6K, a) SEM microstructure of grain boundaries and evaluated carbide particle, b-c) EDS chemical elements mapping, etch. Marble

Generally speaking, SSH only provides strengthening up to approximately 815°C (Sims et al., 1987). Typical elements used in SSH of superalloys are Al, Fe, Ti, Cr, W, and Mo. The use of the more massive elements is desirable because of their lower diffusion rates, but they also increase alloy density and tend to promote the formation of topologically close-packed phases.

A considerable increase in the creep strength of alloys for high-temperature applications can be obtained by precipitation hardening (PH). In the case of Ni-base alloys, this can be achieved using elemental additions such as Ti, Al, and Nb. These elements have limited solubility in the alloy matrix, and the solubility is drastically reduced with a decrease in temperature; therefore, finely distributed precipitates can be generated in the matrix from a supersaturated solid solution during heat treatment.

The precipitates, which are generally coherent intermetallic compounds such as γ'-Ni_3(Ti, Al) or γ''-Ni_3Nb phase, can inhibit the movement of dislocations. Movement of a dislocation in the matrix containing precipitates can only take place by cutting through or by bypassing the particles. The four main factors controlling the effectiveness of PH are (Donachie and Donachie, 2002, Sims et al. 1987):

- Coherency strains between the matrix (γ) and the precipitate (γ', γ'') due to the difference in their lattice parameters.
- Antiphase-boundary (APB) energy in the presence of an ordered precipitate (γ', γ''). The APB represents the energy needed for the dislocation to cut through the ordered precipitate, because cutting could result in disordering between the matrix and precipitate.
- Volume fraction of the precipitate (γ', γ'').
- Particle size.

The last two factors, volume fraction of γ'-Ni_3Al precipitates and particle size was evaluated with coherent testing grid methods. Only reminder, there were evaluated cast alloys ZhS6K and IN 738C due to presence of γ'–phase visible at SEM observation; alloy IN 718 contains at starting stage hard to visible γ'–phase, which become more visible after heat treatment applying – at elevated temperatures above 700°C (see Fig. 8). The number and volume of γ' - phase have significant influence on mechanical properties of these alloys, especially on

creep rupture life. Average satisfactory size of γ′-phase is about 0.35 – 0.45 μm and also carbide size should not exceed size of 5 μm – because of fatigue crack initiation. Another risk of using high temperature loading or annealing is creation of TCP phases, such σ-phase or Laves phase, in range of temperature 750 °C – 800 °C. Results for γ′-phase evaluation (volume fraction, particle size, and number of particles) are presented in Table 2. Exposing for 10/15 hours at annealing temperature the volume of γ′-phase was increased. The most significant increasing in volume of γ′-phase has been observed at ZhS6K alloy where its volume increased from 39.4% to 72.4% (76.6% respectively for 15 hrs. dwell time) what means increasing about 83.7% (94.4% for 15 hrs. dwell time) (Figs. 9a) compared to starting stage. The IN738C alloy does not show such increasing. Also here the γ′-phase increases its volume from 60.4% to 66.6% (71.2% respectively). It is not such dramatic increasing, only for 10.26% (17.88% for 15 hrs. dwell time), compared to starting stage (Figs. 9b).

Table 2
Result for γ′–Ni_3Al phase evaluation at various conditions (own results)

Alloy (condition)	Number of γ′-phase N [μm^{-2}]	Volume fraction of γ′-phase V [%]	The size of γ′-phase u [μm]
Alloy IN 738C			
Start. stage	1.68	60.4	0.76
10hrs./air	1.63	66.6	0.64
15hrs./air	1.58	71.2	0.67
Alloy ZhS6K			
Start. stage	2.47	39.4	0.61
10hrs./air	1.50	72.4	0.69
15hrs./air	1.49	76.6	0.72

Note that the strengthening achieved through coherent strains and ordering increases with particle size, because these two mechanisms require that dislocations cut through the particle. However, Orowan bowing (Koehler et al., 1954), where the dislocation will bypass the particle if it is too large, limits this increase in strength with increasing particle size. The strengthening in this case is provided by the extra work needed for the dislocation to alter its path (Kumar, 1994). The morphology of the coherent precipitate in two-phase alloys is strongly influenced both by the elastic strain energy associated with the lattice mismatch between precipitate and matrix and by the interfacial energy of the particle-to-matrix boundary (Ko et al., 1998). The elastic strain energy depends on the shape, habit, and volume of the precipitates. Interfacial energy merely depends on the surface area of the particle. For a matrix and precipitate with similar lattice parameters, a spherical precipitate is formed, while for large differences in lattice parameters, an elastically favored cuboidal precipitate is formed.

In alloy systems in which SSH elements such as Mo and W have limited solubility, carbides are often used to provide high-temperature strengthening (Kumar, 1994). Carefully designed carbide hardening can be particularly useful for increasing creep strength, because under service loads, the high-temperature creep processes mainly take place at the grain boundaries. Grain evaluation was carried out on wrought superalloys. As an example, the procedure and results for Nimonic 80A alloy samples in the initial condition are presented.

Because the specimens were as wrought, the grain size was evaluated in the longitudinal and transverse directions to the rolling direction.

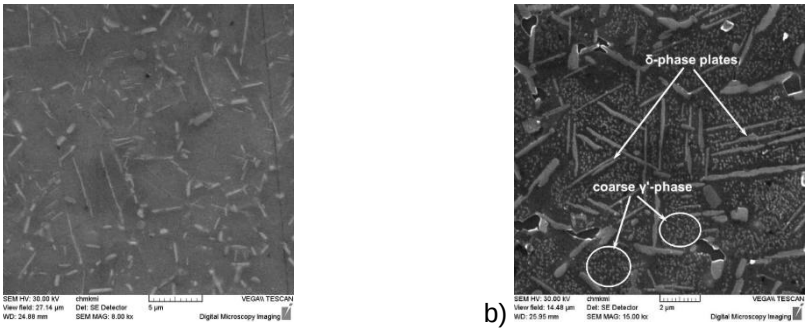

a) b)

Fig. 8. SEM micrographs of IN 718 alloy compared the starting stage (a) to applied heat-treatment at 800°C/72 hrs. (b) Mind the coarse γ'-phase and higher volume of δ-phase plates at grain boundaries and inside grains as well. Etch. 10g CrO_3+100ml H2O (2V,1s,90mA/cm^2)

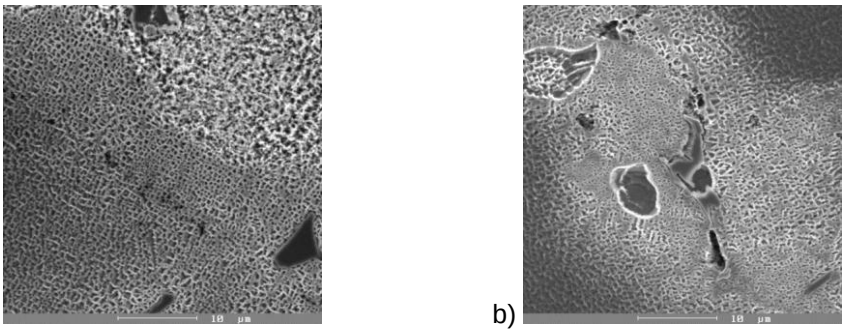

a) b)

Fig. 9. Micrographs for γ′-phase evaluation: a) after 800°C/10hrs cooling on air of ZhS6K alloy; b) after 800°C/10hrs. cooling on air of IN738C alloy, SEM, etch. Marble

Based on the microstructure observation, significant heterogeneity in grain size was found in the surface layers. Along the periphery of the sample, the grain γ-phase was coarse, in the core or at a distance of about 0.358 mm from the surface, the microstructure was already fine-grained, and regardless of whether the sample was observed in the longitudinal or transverse direction.

The grain evaluation was performed in two ways, in accordance with ASTM E112-12.

The first method, evaluation by the planimetric method (Jeffries method). In this method, for example, a rectangle with an area of 5000 mm^2 is considered. This pattern was applied to the microstructure, at least at 5 different locations, and the number of grains that were inside the pattern, N_{inside}, and the number of grains intercepted by the pattern, $N_{intercepted}$, were counted, not counting the grains at the corners of the pattern. The values found were fitted to the equation (1):

$$N_A = \frac{M^2}{A} \times \left(N_{inside} + 0.5N_{intercepted} + 1\right) \quad (1)$$

Where N_A - is the number of grains per mm^2 area at 1x magnification, M - is the applied magnification of the microstructure, A - is the area of the pattern (5000 mm^2), N_{inside} - is the number of grains inside the pattern and $N_{intercepted}$ - is the number of grains intersected by the pattern.

The ASTM value of the grain G is then determined from the table in the relevant standard or it can be calculated from the equation (2):

$$G = 3.321928 \log N_A - 2.954 \quad (2)$$

The second method, evaluation by the linear method or by Heyn. This method uses sections of 500 mm in total length, which are laid out horizontally, vertically and at an angle of 45° in two mutually perpendicular directions on the microstructure. Typically, 5 segments of 100 mm length are chosen, spaced as in Fig. 10a or as described in ASTM E112-12, Fig. 10b. The number of grains intercepted by each line segment is then counted and denoted as "P". Total length of the sections L_T = 500 mm. The actual magnification 'M' shall be recalculated according to the inserted scale. According to equation (3), the mean length of the intersected grains is calculated:

$$\bar{l} = \frac{L_T}{P \times M} \quad (3)$$

The above value is inserted into equation (4) to calculate the ASTM grain size G:

$$G = -6.643856 \log \bar{l} - 3.288 \quad (4)$$

Results for grain size evaluation for Nimonic alloy 80A in starting stage are in Table 3, compared to value given in material sheet provided by alloy supplier.

Table 3
Grain size evaluation results according to ASTM E112-12

Nimonic 80A	Grains N_A [1/ mm^2]	Aver. grain area $\bar{A}$ [μm^2]	Average diameter d [μm]	Mean intercept $\bar{l}$ [mm]	G tab.	G calc.
Grain size according to material data sheet ASTM G = 9.5						
Planimetric (Jeffries) method						
core – trans.	**3968** (1988)	**252** (502.9)	**15.9** (22.4)	-	**9.0**	8.0
surface – trans.	87.82	11385.9	106.7	-	3.5	3.5
Linear (Heyn) method						
core – trans.	1984	504	22.5	0.01894	8	8.16
surface – trans.	175.36	5703	75.5	0.06944	4.5	4.41

(Own measurements. Note: bold values are Table values ASTM E112-12, regular ones (in brackets) are calculated according to given equations)

4. CONCLUSION

Presented contribution provides information how to use OM and SEM techniques at Ni-based superalloys microstructure evaluation. There were presented methods for particle identification as EDS line analysis and chemical elements mapping. The SEM was also used at non-conventional metallography analysis applied on γ' fraction, where was shown the influence of high temperature 800°C and dwell time for 72 hrs. with cooling on air on γ' volume fraction changes. Increasing the γ' size decreasing the high-temperature properties of superalloys. Optical microscopy grain size results shows a quite significant difference to grain size declared by supplier in material sheet, especially on surface area where grain size ASTM were absolutely different ASTM 3-4.5 to guaranteed ASTM 9.5. Speaking in real grain

diameters, the values changes from 129μm-75μm (ASTM G3-4.5) to 13.3μm (ASTM G9.5). Such a significant difference definitively affected the mechanical properties and fatigue life as well.

ACKNOWLEDGEMENTS

The authors acknowledge the KEGA projects No. 004ŽU-4/2023 and No. 009ŽU-4/2023 for the financial support of this work.

REFERENCES

Belan, J., 2012. *Study of advanced materials for aircraft jet engines using quantitative metallography*, Recent Advances in Aircraft Technologies, R., K., Agarwal, Ed., IN-TECH Europe, Rijeka, Croatia, 49-74. DOI: 10.5772/37254

Belan, J., Kuchariková, L., Vaško, A., Tillová, E., 2017. *The influence of high temperature on DV-2 jet engine Ni-based superalloy turbine blade degradation*, Materials Today-Proceedings, 4(5), 5743-5748. DOI: 10.1016/j.matpr.2017.06.039

Dehmas, M., Lacaze, J., Niang, A., Viguier, B., 2011. *TEM Study of High-Temperature Precipitation of Delta Phase in Inconel 718 Alloy*, Advances in Materials Science and Engineering, 2011, 1-9. DOI: 10.1155/2011/940634

Donachie, M., J., Donachie, S., J., 2002. *Superalloys: A Technical Guide*, Materials Park, OH: ASM International Publication, USA.

Durand-Charre, M., 1997. *The Microstructure of Superalloys,* Amsterdam: Gordon and Breach Science, NL.

Furrer, D., Fecht, H., 1999. *Ni-Based Superalloys for Turbine Discs*, JOM, 51(1), 14–17.

Gaddes, B., Leon, H., Huang, X., 2010. *Superalloys – Alloying and Performance*, Materials Park, OH: ASM International Publication, USA.

Ko, H., S., Paik, K., W., Park, L., J., Kim, Y., G., Tundermann, J., H., 1998. *Influence of Rhenium on the Microstructures and Mechanical Properties of a Mechanically Alloyed Oxide Dispersion-Strengthened Nickel-Base Superalloy*, J. Mater. Sci., 33, 3361–3370.

Koehler, J., S., Seitz, F., Read Jr., W., T., Shockley, W., Orowan, E., 1954. *Dislocations in Metals*, M. Cohen, Ed., AIMME, New York, USA.

Kumar, P., 1994. *The Role of Niobium and Tantalum in Superalloys*, Advances in High Temperature Structural Materials and Protective Coatings, A.K. Koul, Ed., National Research Council of Canada, Ottawa, 34–53.

Manriquez, J., A.; Bretz, P., L.; Rabenberg, L.; Tien, J., K., 1992. *The High Temperature Stability of IN718 Derivative Alloys*, Superalloys 1992, S. D. Antolovich et al., Ed., TMS, 507–516. DOI: 10.7449/1992/Superalloys_1992_507_516

Pollock, T., M.; Tin, S., 2006. *Nickel-Based Superalloys for Advanced Turbine Engines: Chemistry, Microstructure, and Properties*, Journal of Propulsion and Power, 22(2), 361-374. DOI: 10.2514/1.18239

Reed, R., C., 2006. *The Superalloys: Fundamentals and Applications,* New York, NY: Cambridge University Press, USA.

Sims, Ch. T., Stoloff, N., S., Hagel, W., C., 1987. *Superalloys II – High-temperature materials for aerospace and industrial power – 2nd Edition,* John Wiley & Sons, New York, NY, USA.

Sundararaman, M.; Mukhopadhyay, P.; Banerjee, S., 1992. *Some aspects of the precipitation of metastable intermetallic phases in INCONEL 718*, Metallurgical transactions. A, 23(7), 2015–2028. DOI: 10.1007/BF02647549

Sunulahpašić, R., Oruč, M., Hadžalić, M., Rimac, M., 2012. *Optimization of the mechanical properties of the superalloy Nimonic 80A*. Materials and Technologies, 46(3), 263-267.

Vaško, A., 2016. *Evaluation of shape of graphite particles in cast irons by a shape factor*, Materials Today-Proceedings, 3(4), 1199-1204. DOI: 10.1016/j.matpr.2016.03.006